Metrol. Meas. Syst., Vol. 31 (2024) No. 3, pp. 511–528
DOI: 10.24425/mms.2024.150283

PAN POLSKA AKADEMIA NAUK

METROLOGY AND MEASUREMENT SYSTEMS
Index 330930, ISSN 0860-8229
www.metrology.wat.edu.pl

M&MS

CRACK DETECTION OF HIGH-STRENGTH WIND TURBINE BOLTS BASED ON FIBER BRAGG GRATING SENSORS

Yu-Tao Chen[1)], Peng Zhou[2)], Li-Yun Chen[2)], Guo-Qing Gu[3)], Li-Ya Dai[3)], Yong-Qing Wang[4)]

1) School of Electrical Engineering, Yancheng Institute of Technology, Yancheng 224051, China
2) Yancheng Institute of Supervision & Inspection of Product Quality, Yancheng 224056, China
3) School of Civil Engineering, Yancheng Institute of Technology, Yancheng 224051, China (✉ *gqgu@ycit.edu.cn*)
4) School of Electrical Engineering, Yancheng Institute of Technology, Yancheng 224051, China

Abstract

With the rapid development of the wind energy industry, there is an increasing concern about operation safety and reliability of high-strength wind turbine bolts. The aim of this paper is to monitor the strain change around the cracks in wind turbine bolts by means of fiber Bragg grating (FBG) sensors for crack detection. Firstly, the strain distributions of wind turbine bolts' cracks with different locations and angles in the service condition are simulated using finite element analysis (FEA). Then, three-point grating string FBG sensors were pasted on the surface of wind turbine bolts with fatigue cracks to monitor the strain changes around the cracks in real time. By analysing the monitored strain data elaborately, the location of the crack on the bolt surface was successfully detected by identifying the location of the maximum strain detected by FBG sensors. In addition, the strain distributions in the vicinity area of the crack at different angles (0°, 45°and 90°) were also monitored and analysed in depth. The different types of crack angles could be distinguished based on of different strain distribution of the vicinity of the crack tip at different angles. The experimental results show that the FBG sensing technology has a high degree of sensitivity and accuracy in crack detection of high-strength wind turbine bolts.

Keywords: Wind turbine bolts, crack detection, fiber Bragg grating, finite element analysis.

1. Introduction

In recent years, wind power has become the fastest growing new energy industry in the world [1]. Chinese wind power is developing rapidly, and the annual new installed capacity in the past decade or so is close to 40%–50% of the global total, which has made China the largest and fastest growing country in the world in terms of wind power generation [2–4]. However, with the rapid development of the wind power industry, the pressure of operation and maintenance of wind turbines has gradually increased, and a variety of mechanical failures and accidents have entered a high incidence period [5]. Online monitoring of key equipment and structural components of

Article history: received January 11, 2024; revised April 5, 2024; accepted April 9, 2024; available online June 12, 2024.

wind turbine generators (WTGs) has become the focus of the industry's attention, of which the bolted connection is one of the most important connection methods in WTGs. Once the bolt connection structure fails or fatigue cracks appear, it will seriously affect the quality, safety and operational reliability of a WTG [6–8].

Commonly used crack detection methods for wind turbine bolts include visual inspection, ultrasonic guided wave method, acoustic infrared imaging method and resistance strain detection, *etc.* The ultrasonic guided wave method solves the problem of traditional visual inspection being time-consuming and laborious. When the guided wave propagates in the connecting structure and encounters boundaries or defects, the reflected wave returns. By using signal processing technology to detect the received signal, the position and size of structural cracks can be detected. Wagle *et al.* [9] employed the surface wave technology to detect the aluminium alloy plate bolted connection structure of the cracks in the sprouting and expansion, and found that the bolt holes before the region of the scattered wave intensity increased with the fatigue degree of the connection structure. However, the ultrasonic wave guide method was usually suitable for bolt crack detection only when WTGs were stopped for the examination. Subsequently, many new fast and accurate crack detection methods for wind turbine bolts have emerged. Zhu *et al.* [10] found that the thermal response of cracks increased with crack length, which provided a strong basis for quantitative identification of bolt crack length. In addition, Hasni *et al.* [11] developed a hybrid network of electrical strain and acceleration sensors, which can accurately detect cracks on bolted structural members by arranging the sensors in the inspection area, thus realizing effective bolt crack detection.

Fiber Bragg grating (FBG) sensors have made remarkable progress in wind turbine bolt detection in recent years, with gradual improvement in accuracy and stability. The FBG sensor possesses the advantages of light weight, small size, high sensitivity, and strong resistance to electromagnetic interference [12], so it has received more and more attention in the field of structural health monitoring [13], and is widely used in the fields of offshore wind power, ships, bridges, and aviation [14–16]. Currently, the most used strategy is to use FBG sensors to monitor the strain on the health of large structures to assess their service condition, thus ensuring their safe operation. Sah R.K. *et al.* [17] designed an optical displacement sensor based on FBG for crack monitoring with temperature compensation. The sensor achieves accurate quantitative identification of cracks width in large industrial structures by accurately observing the time delay between the output pulse and the reference FBG at different displacement values, which in turn enables accurate quantitative identification of cracks width in large industrial structures. Dai T. *et al.* [18] developed an innovative crack extension width measurement device based on FBG sensing technology, which is specifically designed for monitoring the extension of cracks under alternating load, and has demonstrated its performance in crack damage monitoring of oceanic platforms. It exhibits a high degree of linearity and repeatability, which plays a crucial role in ensuring the safety and health of marine structures. Bao *et al.* [19] constructed a monitoring model by combining a variety of damage recognition algorithms, such as neural networks, and proposed an FBG-based anti-noise interference crack damage detection method, which can detect the depth and radius of cracks in reinforced structures.

In metal crack detection, FBG is often applied to monitor micro cracks in aluminium alloy plates during fatigue. Jin *et al.* [20] compared the performance of *apodized FBG* (AFBG) and *uniform FBG* (UFBG) sensors used for structural crack propagation monitoring in the crack extension process of aluminium alloy plates with aperture-edge cracks, and found that the UFBG sensors were more sensitive to capturing the crack extension lengths than the AFBG sensors. Zhang *et al.* [21] analysed the performance of two damage features, *full-width at half-maximum* (FWHM) and spectral difference and found that they show extremely high sensitivity to the complex strain field induced by grain extension, and can be applied to quantitatively identify the crack location

during the crack extension process. Sun *et al.* [22] used fatigue loading experiments to obtain the response characteristics of loading times and crack lengths to the peak-to-peak values of FBG wavelengths, which not only performed the identification of crack locations, but also predicted the lengths of fatigue crack extensions using the gradient boosting regression tree algorithm. Although the study above provides an important basis for the visualization and detection of fatigue cracks in wind turbine bolts, there are still some shortcomings. Among them, the most significant one is lack of accurate identification of crack location in wind turbine bolts and inability to recognize different angles of cracks with strain laws.

This paper mainly discusses the method of adhesive encapsulation to paste the FBG sensor around the crack tip of the wind turbine bolt with crack defects. The wind turbine bolt crack detection under an axial tensile load is implemented by monitoring the strain distribution around the crack tip with FBG sensors, and analysing the change rule of the strain to determine the location and angle information of the cracks. This method provides a reference for identification of crack characteristics of wind turbine bolts and helps to improve the reliability and safety of wind power equipment.

2. Crack Strain FBG Monitoring Principle

2.1. Brief Synopsis of FBG Sensing Principle

The FBG sensor is a widely used wavelength-modulated optical fiber sensor renowned for its capability to monitor temperature and axial strain. The fiber grating reflects light signals at a precise wavelength when the Bragg wavelength condition is met, that is, when the wavelength of the incident light precisely matches twice the period of the grating. All other wavelengths are permitted to pass through without interruption. This phenomenon can be mathematically expressed as [23],

$$\lambda_B = 2n_{\text{eff}}\Lambda, \tag{1}$$

where λ_B is the central wavelength, n_{eff} is the effective refractive index of the fiber grating, and Λ is the period of the grating.

By measuring the offset of the Bragg wavelength, the change in temperature or strain at the grating can be obtained. This is because FBG sensors are highly sensitive to temperature and strain changes. If external temperature change can be ignored, the relationship between the Bragg wavelength offset and the axial strain change can be expressed as [24],

$$\Delta\lambda_B = \lambda_B(1 - p_e)\Delta\varepsilon, \tag{2}$$

where $\Delta\lambda_B$ is the Bragg wavelength offset, λ_B is the initial Bragg wavelength, p_e is the elasto-optical coefficient, $\Delta\varepsilon$ is the axial strain variation.

Therefore, it can be assumed that there is an approximate linear relationship between the Bragg wavelength offset and the axial strain, making the FBG an effective sensing tool for measuring the axial strain.

2.2. Basic Theory of Crack Propagation

In Fracture Mechanics problems, when axial load is applied to the bolt, the calculation of strain at the crack is determined by the type and location of the crack. The crack can be categorized into three distinct modes based on its location: open mode (Mode I), slip mode (Mode II), and tearing mode (Mode III) [25, 26]. Among these modes, open mode is the most common and intuitive form of cracking. This paper focuses primarily on the strain around the open mode.

In an elastic material devoid of cracks, the correlation between stress and strain adheres to Hooke's law. Nevertheless, when cracks are present, the material demonstrates a stress singularity in the crack tip region, necessitating the introduction of a stress intensity factor, K_I, to represent the magnitude of the stress field in that specific area [27, 28],

$$K_I = F\sigma\sqrt{\pi \mathrm{a}}, \tag{3}$$

where σ is the stress, a is the length of the crack perpendicular to the stress direction, and F is the geometric correction factor, which depends on the shape, size, and location of the crack as well as the geometry.

For an ideal linear elastic material, the strain distribution at point r from the crack tip after being subjected to an axial tensile load in the presence of a crack on the bolt surface can be calculated by means of fracture mechanics [29],

$$\varepsilon(r) = \frac{K_I}{\sqrt{2\pi r}}, \tag{4}$$

where $\varepsilon(r)$ is the strain at point r from the crack tip, K_I is the stress intensity factor for Type 1 cracks, r is the distance from the crack tip to the point under consideration.

According to Eq. (4), the magnitude of strain at point r is inversely related to its distance from the crack tip. The strain is highest in the vicinity of the crack tip due to the concentration of stress at this location. As the distance from the crack increases, the strain diminishes, as the stress distribution across the bolt becomes more uniform, leading to a corresponding decrease in strain.

By combining Eqs. (3) and (4), it can be inferred that at the same distance r from the crack tip, a radial crack produces a larger strain than an axial crack. This is because for radial cracks, their length is perpendicular to the stress direction, leading to a larger effective stress length. Conversely, the effective stress length for axial cracks is limited to the width of the crack, resulting in a smaller effective stress length. As a result, axial cracks exhibit a lower stress concentration, leading to a more uniform strain distribution and relatively small strain around the crack.

As for a 45° angle crack, it is essential to consider the stress intensity factors of both modes simultaneously. Specifically, the stress intensity factor for Mode I is directly related to the vertical tensile stress experienced by the crack, while the stress intensity factor for Mode II is associated with the shear stress experienced by the crack. To accurately represent the strain distribution in the vicinity of the crack, the *finite element analysis* (FEA) method can be utilized to simulate the stress field in the region surrounding the 45° crack.

3. Finite Element Analysis

3.1. Model Establishment

In this section, a 1:1 scale bolt crack damage model was created using SolidWorks software. The model was created to simulate an M42# wind turbine bolt, featuring the following dimensions, diameter d = 42 mm, screw length l = 250 mm, thread length b = 100 mm, the prefabricated crack had a circumferential length s = 47 mm, width w = 2.5 mm, and depth h = 3 mm. These dimensions and details are illustrated in Fig. 1.

To simulate the strain distribution around the bolt crack, the *finite element analysis* (FEA) software ABAQUS was utilized. The material properties of the specimen are presented in the table and are assumed to be uniform and isotropic. The bolt was fixed at the bottom, and a peak axial

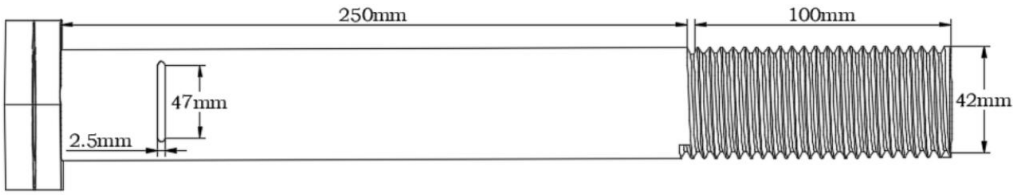

Fig. 1. Diagram of bolt's component dimensions.

tensile load of 435 MPa is applied to the head. For mesh generation, a global mesh size of 10 mm was defined, with locally refined meshing at the edge of the crack. The refined mesh size was set to 1 mm, and a tetrahedral mesh was utilized for the bolt specimen. Table 1 lists the detailed material properties of the tested bolt specimen.

Table 1. Material properties of the tested bolt specimen.

Property	**Parameter**
Material type	42CrMo
Young's modulus (Pa)	2.12 × 1011
Poisson's ratio	0.28
Density (kg/m3)	7850
Performance level	10.9
Tension strength (MPa)	≥ 1040
Yield strength (MPa)	≥ 940
Elongation after fracture (%)	≥ 9
Shrinkage after fracture (%)	≥ 48

3.2. Simulated Results

Fig. 2 presents the strain field simulation results of the bolt with transverse cracks located at different positions under the same axial tensile load of 600 kN. It is evident that there is a stress concentration region in the vicinity of the crack tip, exhibiting the crack tip singularity of the strain field. The strain distribution cloud maps indicates that the strain value of the bolt gradually decreases as the distance from the crack increases, agreeing with the previous theoretical predictions. Additionally, the law of the strain field provides valuable guidance for determining the location of bolt cracks.

Taking the example of the presence of cracks in the bolt in Fig. 2a, three axially equally spaced points A, B and C in the bolt in Fig. 2a were selected and taken into consideration. The relationship curves between strain distribution at Points A, B and C and the axial load are plotted in Fig. 3. By comparing the strain-load curves of Points A, B and C in the finite element simulation, it is found that the strain growth rate at Point A is the most significant. When the load reaches the peak value of 600 kN, the strain at point A has the maximum value, followed by Point B, while the strain at Point C is the smallest. This phenomenon indicates that the closer the distance to the crack, the greater the strain generated in the bolt when subjected to axial load.

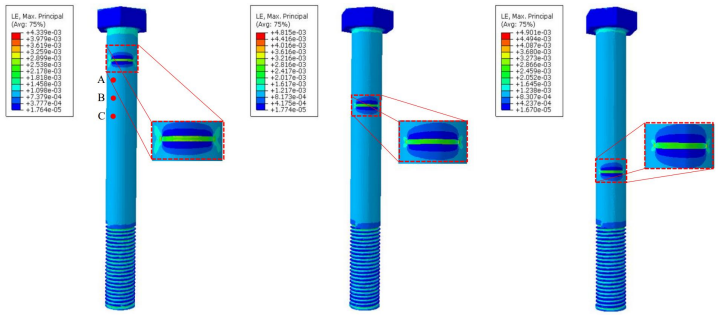

Fig. 2. Crack tip strain FEA cloud maps at different locations under 600 kN load.
(a) upper, (b) middle, (c) bottom.

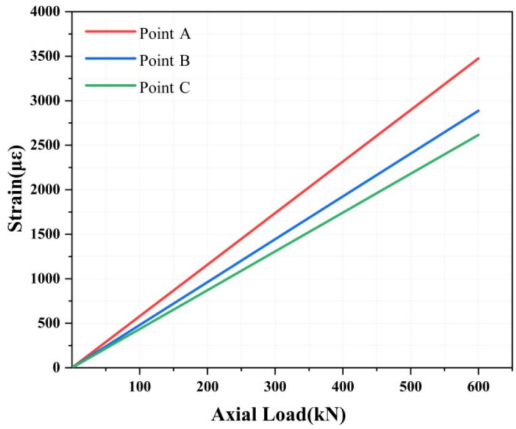

Fig. 3. Numerical calculation strain distributions at three different points.

The strain field simulation results for the bolt with different angle cracks at the same position, after being subjected to the same axial tensile load, are presented in Fig. 4. It is observed that a stress concentration phenomenon exists in the region near cracks at various angles. Furthermore, the strain distribution cloud maps reveal the maximum principal strains generated around cracks at different angles. Notably, the strain around the 90° crack is the smallest after application of the axial tensile load, followed by the 45° crack, with the maximum strain occurring around the 0° crack. This finding agrees with the theoretical analysis presented in the previous section. Additionally, this law of the strain field suggests that the crack angle can be inferred by monitoring the strain near the bolt crack.

In the finite element simulation results in Fig. 4, the same point D in Fig. 4a~4c was selected and taken into consideration. As shown in Fig. 5, the load-strain curves at point D with different angles of cracks are similarly plotted as an example of point D, which is closest to the crack. After being subjected to axial load, the maximum strain was generated near the 0° crack, followed by the 45° crack, while the 90° crack had the smallest strain. It is suggested that by monitoring the strain near the crack, it is possible to identify the different angles of the crack.

In summary, the simulation results of bolts with cracks at various locations and angles under axial tensile loading were obtained through finite element simulation. It can be seen that stress concentration phenomena of varying degrees occur at the crack tips. This stress concentration effect

Metrol. Meas. Syst., Vol. 31 (2024), No. 3, pp. 511–528
DOI: 10.24425/mms.2024.150283

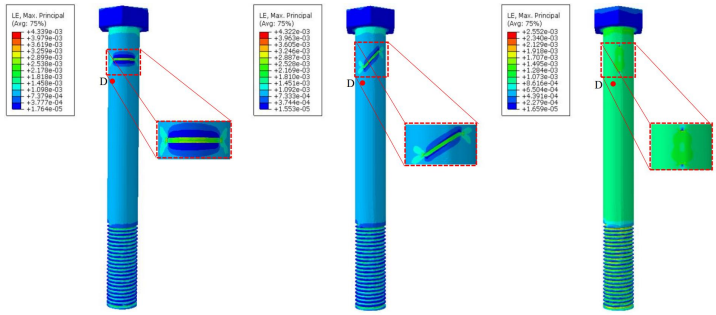

Fig. 4. Crack tip strain FEA cloud maps at different angles under 600 kN load. (a) 0°, (b) 45°, (c) 90°.

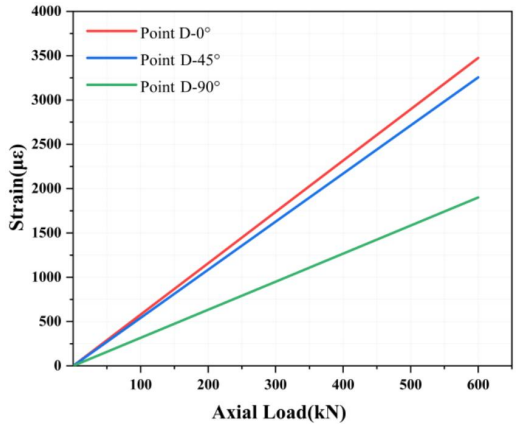

Fig. 5. Numerical calculation strain distributions at the same three points with different angles.

significantly increases the strain level at the crack tips, which can facilitate more accurate determining of the location of the crack. Additionally, by analysing the strain values of cracks with different angles at the same location, it can be found that the smaller the crack angle, the higher the strain at its crack tip. These conclusions will provide an important reference for subsequent experiments.

4. Experiments

This section presents experimental investigations conducted with the proposed FBG-based methodology for crack detection of the high-strength wind turbine bolts. The practical wind turbine bolt test with applying axial tensile load was carried out to verify the feasibility and effectiveness of the proposed FBG-based bolt crack detection method.

4.1. Preparation of Bolt Specimens

The experimental bolt specimens were M42# Dacromet wind turbine bolts with hot dip galvanizing, which were made of 42CrMo high-strength steel, and had a nominal diameter of 42 mm and a performance level of 10.9. The specific material properties are listed in Table 1.

Firstly, various cracks at both different positions (bottom, middle and upper) and angles (0°, 45° and 90°) at the screw surface were prefabricated by a laser cutter so as to obtain a series of bolt specimens with cracks. It is worth emphasizing that the laser cutter was used here to fabricate the artificial bolt cracks to simulate the real bolt cracks. However, compared with the real fatigue crack, the laser cutting of the formation of the crack is relatively flat and regular, the crack angle can be controlled, and the width of the crack is relatively large, while the real fatigue crack is generally formed at random angles between 0° and 90°, and has a small width, rough and uneven surfaces, and tends to show irregular shapes. Despite of these minor differences, both two types of cracks share the same experimental laws. Therefore, the detection of the artificial bolt cracks can provide a valuable guidance for the detection of real bolt cracks. Then, the three-point string FBG sensors were adhered near the prefabricated cracks at each bolt specimen using the adhesive encapsulation method. The specific adhesive encapsulation process involves the following steps, as shown in Fig. 6,

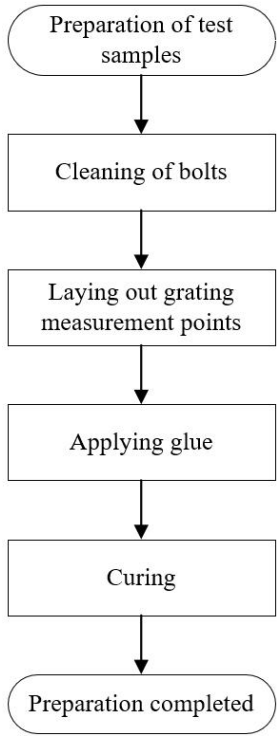

Fig. 6. Preparation flow chat of the test specimens.

Step 1: Cleaning of bolts. Applying cleaner to the surface of bolts and rinsing with water to remove oil from the surface of the bolts.

Step 2: Laying out grating measurement points. Although more precise signals can be achieved by positioning the grating points closer to the crack, it is better to avoid placing the grating points too close to the crack tip. According to the finite element simulation results and the sensors' survivability requirement, the grating point located 10mm away from the tip of the crack seems to be the best choice.

Step 3: Applying glue. Tapes were used to fix both ends of the grating on the surface of the bolt screw. Then, YH-840B glue was applied to paint uniformly on each grating measurement point. The entire painting process should ensure that the thickness of the adhesive layer is uniform. Considering that the length, width and thickness of the adhesive layer has an important effect on the strain transfer [30], the optimized adhesive layer is of the length 12 mm × width 4 mm × thickness 0.5 mm [31].

Step 4: Curing. The bolt specimens coated with YH-840B glue were cured naturally at room temperature of 25° for 5 hours.

By means of the above-mentioned fabrication process, five bolt specimens were prepared for testing. Three bolt specimens with 0° crack, prefabricated at upper, middle, and bottom parts of the specimens respectively, were used for crack location identification experiments, and the other two specimens with 45° and 90° cracks, located in the upper part of the bolts, were used for crack angle detection experiments. It is worth noting that the 0° crack specimen located in the upper part was the common shared specimen in the two sets of experiments to explore the location and angle of the cracks. One of the prepared bolt specimens was illustrated in Fig. 7.

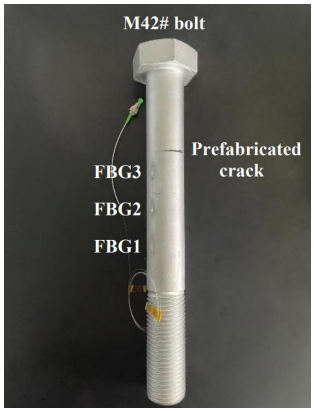

Fig. 7. One of the prepared bolt specimens.

The adhesive encapsulation process significantly impacts the Bragg wavelength. The wavelengths of three gratings were detected both before and after pasting the grating, revealing a "blue shift" of approximately 0.3 nm in the Bragg wavelengths of the three measurement points. However, there were no significant changes in the reflectance spectra's peaks and valleys. This "blue shift" was primarily attributed to the symmetrical distribution of residual stress on the optical fiber resulting from the adhesive encapsulation process. Nevertheless, this shift cannot compromise the integrity of subsequent experiments.

4.2. Experimental process

To ensure the accuracy of the experiment, the entire process was implemented at room temperature to minimize the impact of temperature variations on the FBG sensors' centre wavelength. The experimental setup for tensile testing and strain monitoring was shown in Fig. 8, including an MTS 3000 kN tensile test machine, M42# wind turbine bolt specimens, three-point grating string FBG sensors, a TV1600 FBG demodulator with an accuracy of 1pm (by Beijing Tongwei Co., Ltd.), and a computer.

Fig. 8. The experimental setup for bolt crack detection.

The displacement-controlled method was employed to perform uniaxial tensile and graded loading tests on the bolt specimens. The loading speed was set at 2mm/min, and the real-time tension force was displayed via the machine's force sensor. Each level of loading spanned from 0 kN to100 kN, up to a maximum of 600 kN. After completing each level of loading, the test machine maintained the load for 100 seconds to allow the bolt's elongation to stabilize. It enabled us to record multiple Bragg wavelength data, which were then averaged. During the experimental process, each specimen was repeatedly tested three times.

During the loading process, the FBG demodulator continuously monitored the Bragg wavelengths of the FBG sensors at three grating measurement points. Once the final level of loading was completed, the demodulator stopped the wavelength acquisition and the test machine then unloaded the specimen.

5. Results and Discussions

5.1. Crack Locations Detection

During this experiment, the bolts were cracked at three different locations with same angle under the same axial tensile load. Multiple sets of Bragg wavelengths from the FBG demodulator were recorded and averaged at each level of loading. To obtain the strain data of the measurement points around the bolt crack tip, it was necessary to convert the recorded wavelength data of each FBG into strain data. It is important to note that all FBG sensors used herein had a strain sensitivity coefficient of 1.2 pm/$\mu\varepsilon$. The specific strain values of each FBG under different loads are presented in Fig. 9.

It can be obviously observed from Fig. 9 that there is a linear relationship between the imposed loads and the measured strain values, indicating high accuracy of the FBG sensors for strain monitoring. When the crack was located near FBG1, FBG2, and FBG3, respectively, the FBG sensor closest to the crack exhibited the highest strain value. As the distance between the crack and the sensor increased, the strain values measured by the remaining two FBG sensors decreased sequentially. This observation confirms the stress concentration effect at the crack tip, as described in Fig. 3.

Metrol. Meas. Syst., Vol. 31 (2024), No. 3, pp. 511–528
DOI: 10.24425/mms.2024.150283

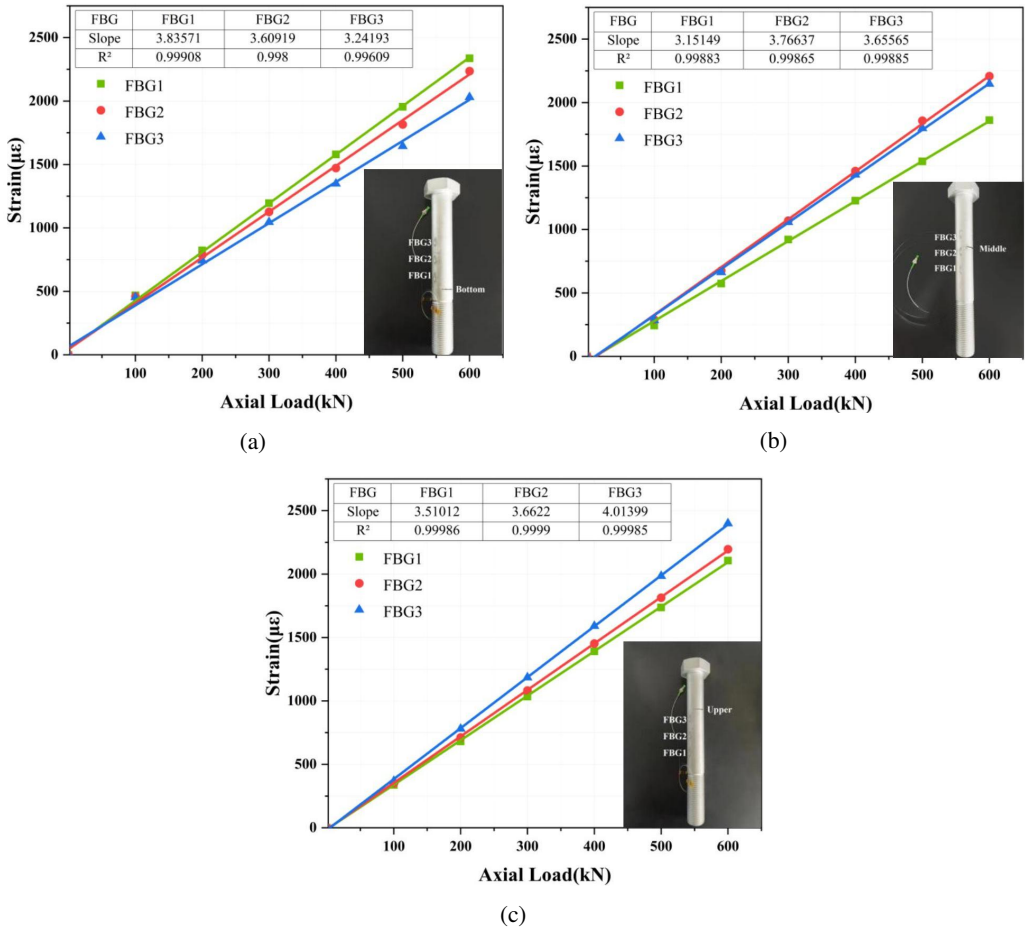

Fig. 9. Bolt crack tip strain distribution at different locations.
(a) bottom, (b) middle, (c) upper.

Additionally, by comparing the slopes of the individual FBG measurement point curves in Fig. 9a, 9b, and 9c, it can be observed that the slope of the FBG measurement point curve nearest to the crack is the steepest, indicating that the strain generated in this FBG region is greater. Therefore, by comparing the magnitudes of the slopes of the load-strain curves measured at the FBGs surrounding the crack tip, it is possible to determine the exact location of the crack.

However, it can be seen from Fig. 9 that the slopes of the curves of the three measurement points are very closer to each other when the load is below 200 kN, and it is not easy for naked eye to distinguish the strain magnitude of each measurement point. Therefore, to observe the strain pattern more intuitively, the first-order backward difference is used to describe the strain change rate [32,33],

$$\Delta\varepsilon_k = \varepsilon_k - \varepsilon_{k-1}, \tag{5}$$

where $\Delta\varepsilon_k$ is the strain gradient, ε_k is the strain at the current level load, ε_{k-1} is the strain at the previous level load. As a result, the strain gradient distribution at each measurement point under axial tensile loading for cracks at different locations is as shown in Fig. 10.

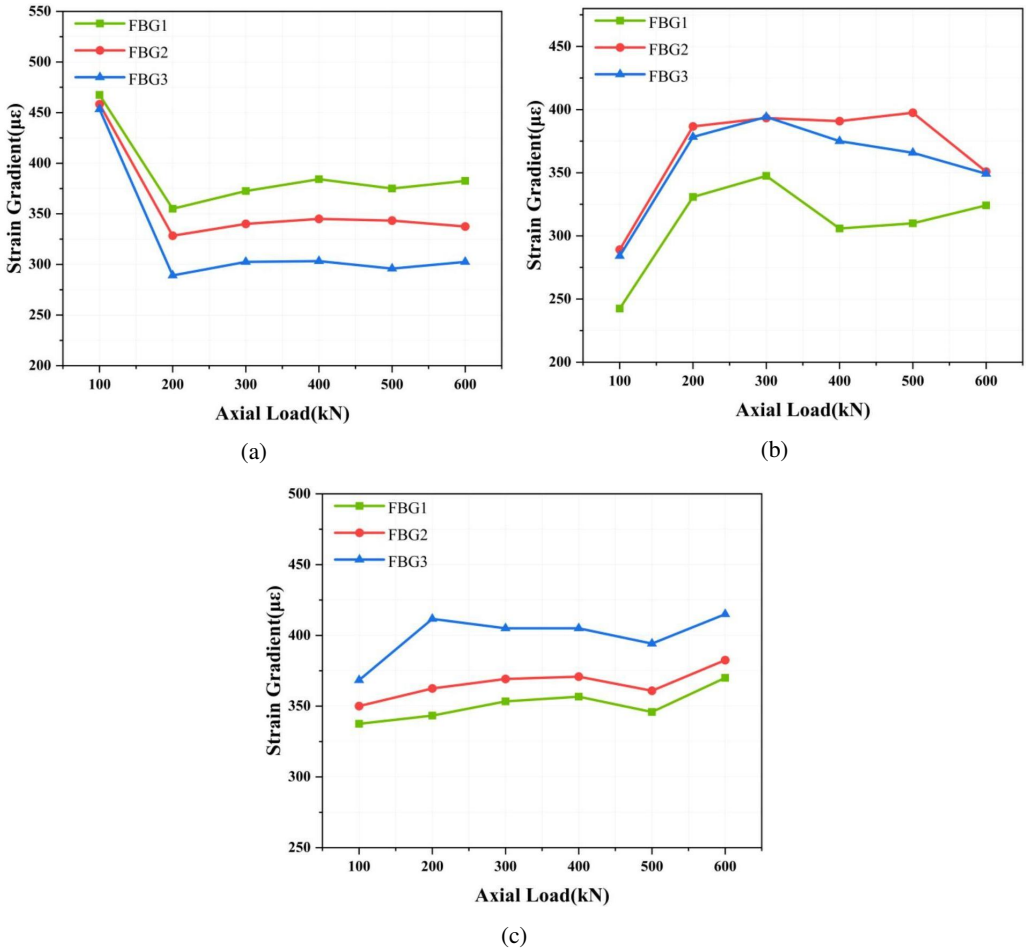

Fig. 10. Bolt crack tip strain gradient distribution at different locations.
(a) bottom, (b) middle, (c) upper.

It can be indicated from Fig. 10 that when cracks appear near FBG1, FBG2, and FBG3, respectively, the strain gradient corresponding to the FBG measurement point closest to the crack is the highest, and the strain changes most rapidly at this FBG measurement point. Therefore, it can be inferred that the crack exists in the vicinity of the FBG measurement point with the highest strain gradient. As previously described in Eq. (4), the magnitude of strain at a point r is inversely proportional to its distance from the crack tip. The strain reaches its maximum around the crack tip, where the stress is highly concentrated. As the distance from the crack increases, the strain decreases. This is primarily because that the stress distribution in the bolt becomes more uniform away from the crack, resulting in a corresponding decrease in strain. During the experiment, it was observed that the wavelength measured at the FBG measurement point closest to the crack had a more significant increase in wavelength compared to the other two FBG measurement points. This further supports the conclusion that the crack is located near the FBG measurement point with the highest strain gradient.

However, upon comparing the strain gradient plots of Fig. 10a, 10b, and 10c, it is evident that the strain gradient curves of each FBG measurement point in Plots (a) and (c) display a more distinct spacing. In contrast, the strain gradient curves of FBG2 and FBG3 in Plot (b) align more closely. This observation is attributed to the fact that during the prefabrication of the crack, to prevent stress concentration at the crack tip from causing damage to the grating at the FBG2 measurement point during the tensile process, the crack position was deliberately deviated upward or downward from FBG2. In this experiment, a 10 mm upward deviation of the crack position was chosen. Given the layout of the FBGs, the FBG3 measurement point is situated 25 mm away from the FBG2 measurement point, leading to a closer alignment of the measured strain gradient changes between FBG2 and FBG3.

5.2. Crack Angle Detection

The actual strain values around the crack at each level of loading measured at each FBG for the bolts with different angular cracks at FBG3 position under the axial tensile load are shown in Fig. 11.

In Fig. 11a and 11b, the load-strain curves for both 0° and 45° cracks demonstrate that the slope measured by FBG3 is higher than those of the other two FBGs, confirming the previous conclusion that the crack location can be inferred by comparing the slopes of load-strain curves from different FBG sensors. However, for the 90°crack, the surrounding strain distribution is different from the strain distribution corresponding to 0° and 45° cracks. Since the crack runs parallel to the tensile load direction, Eq. (4) indicates that the effective axial tensile load acting on the 90° crack is equivalent to its width. As seen in Fig. 3, the stress concentration at the crack tip is minimal, leading to a relatively uniform strain distribution around it. Consequently, the strain values measured by all three FBGs are similar. In Fig. 11c, the slope of the FBG1 curve is slightly steeper than the other two FBGs. This is because, in the bolted joint structure, besides crack damage, the threads act as a weak point of the bolt. Upon tensile loading, strain develops at these threads, influencing the closest FBG1 sensor, leading to its highest strain measurement.

In practical applications of wind turbine bolts, fatigue cracks often initiate at an angle of 45° in bolts that are in service. This occurs because the bolt undergoes cyclic stress or strain, and the crack follows the direction of maximum shear stress at an angle of 45° to the surrounding expansion. On the other hand, 90° cracks are generally not observed in service, and they are often due to improper operation during bolt manufacturing or installation. They may be related to the bolt's internal structure, processing technology, or stress concentration during installation. Bolts with 90° cracks exhibit more uniform strain distribution around the crack, indicating less impact on its performance. Since 90° cracks generally do not cause stress concentrations in service, they have minimal effects on the bolt's load-bearing capacity.

Meanwhile, the identification of different angles of cracks is also analysed with the help of strain gradient. Figure 12 compares the strain gradient of FBG at the same position in the specimen with cracks at different angles.

After comparing the strain gradients of cracks at different angles measured at the three FBG points while maintaining the sensor layout, it was observed that the strain change at the 0° crack tip was the largest at the corresponding position of the FBG. This indicates that when the crack is perpendicular to the applied load direction, the FBG sensor detects the fastest strain rate around the crack. Secondly, the strain change at the 45° crack tip was also relatively large, indicating that when the crack is at an angle of 45° to the applied load direction, the rate of strain changes around the crack detected by the FBG sensor is second only to the case of 0° crack. Whereas, the strain change at the tip of the 90° crack is the smallest. This is because the 90° crack direction is parallel to the applied load direction, and the stress concentration effect at the crack tip is not significant. By comparing the strain changes of FBG sensors under different angles of cracking, it is possible

to roughly determine the angle of cracking and assess its impact on the health of wind turbine bolts. This provides a more accurate and effective monitoring method for the maintenance and overhaul of wind power equipment.

In total, the experimental results above suggest the potential of using FBG sensors to monitor the health of wind turbine bolts by identifying the location and angle of cracks. When a bolt experiences cracking, the strain near the crack changes, leading to changes in the wavelength measured by the FBG sensor. By analysing the rate of change in the FBG wavelength, it is possible to detect the location and angular characteristics of crack appearance. Furthermore, the experimental results have a good agreement with the FEA simulation results, providing further confirmation and enhancing the reliability of these conclusions. This study offers robust theoretical and practical support for the application of FBG sensors in bolt health monitoring and crack localization in future wind farm operations.

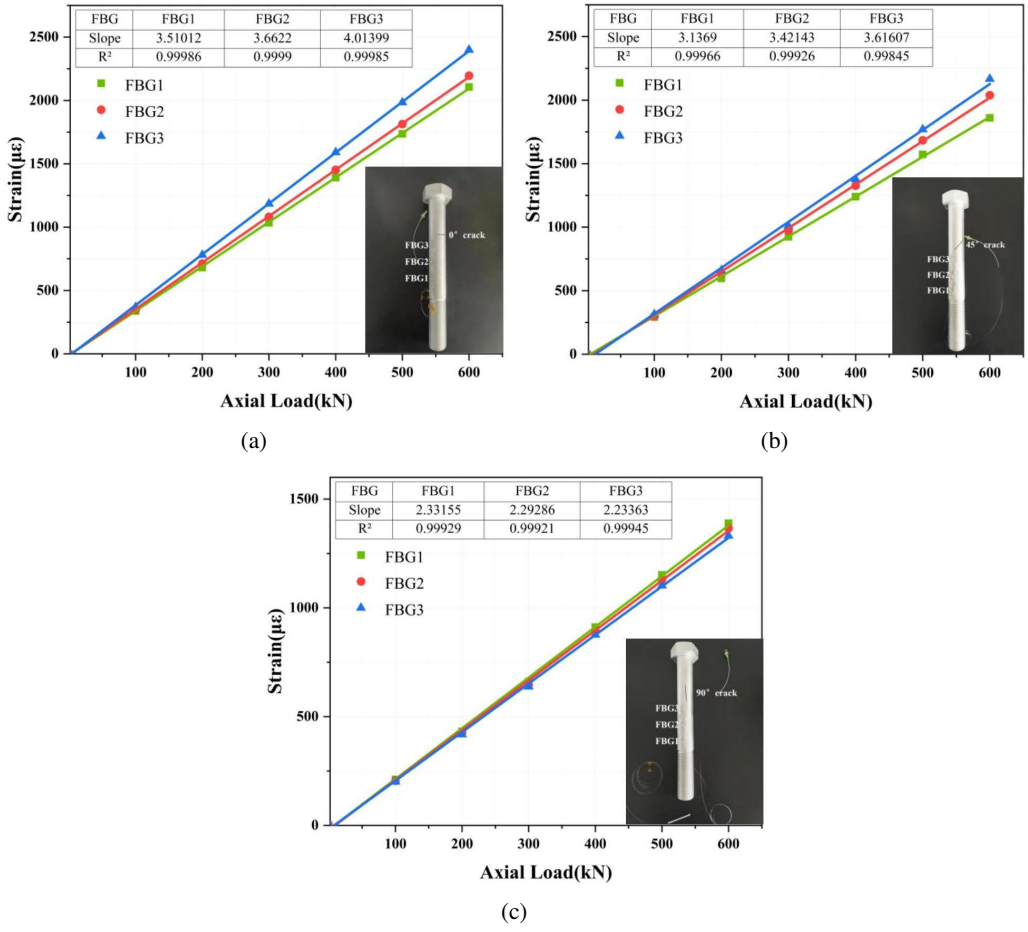

Fig. 11. Bolt crack tip strain distribution at different angles.
(a) 0°, (b) 45°, (c) 90°.

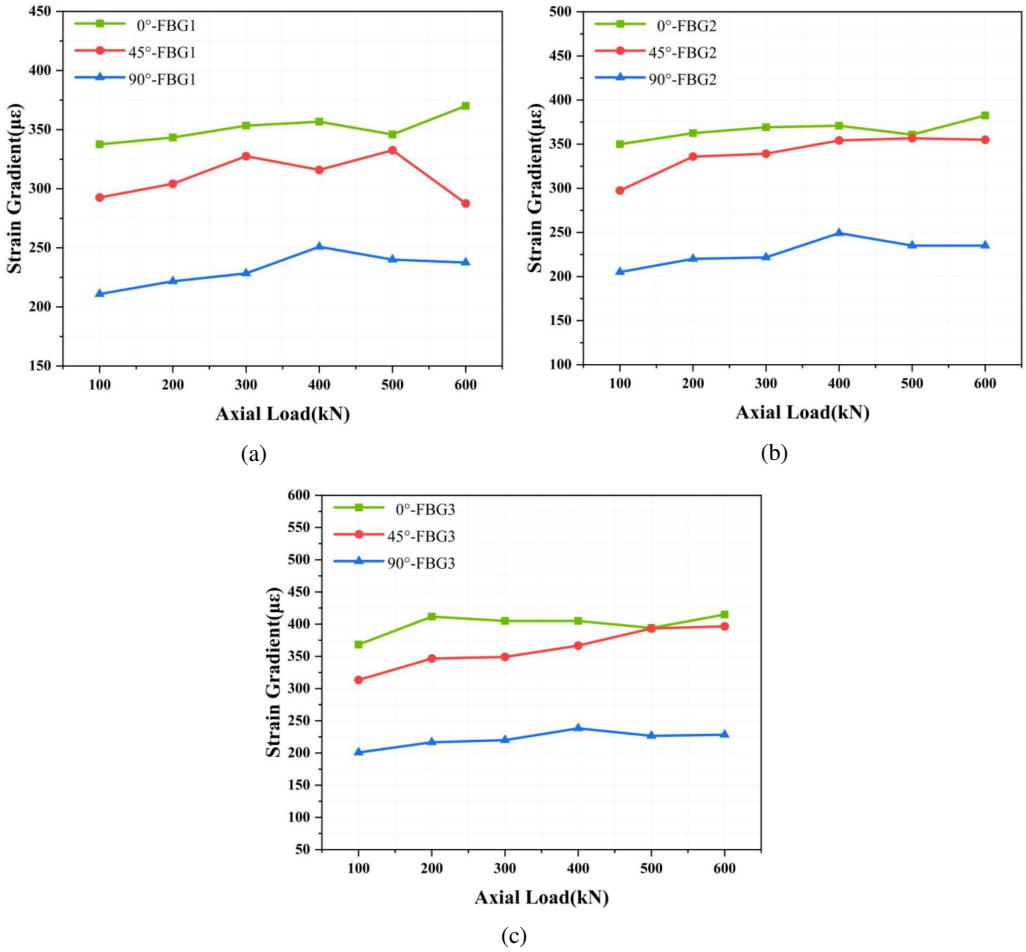

Fig. 12. Bolt crack tip strain gradient distribution at different angles.
(a) FBG1, (b) FBG2, (c) FBG3.

6. Conclusions

In this paper, the finite element method was firstly employed to simulate the strain field variations around wind turbine bolt cracks under axial tensile loading, considering different crack locations and angles. To accurately monitor these strain patterns, an adhesive encapsulation technique was utilized to attach the three-point grating string FBG sensors to the vicinity of the bolt crack. Experimental validation has revealed that the strain change is most significant at the crack tip, decreasing gradually with increasing distance from the crack, the crack location can be quantified by determining the location of the maximum strain detected by the FBG. Furthermore, the angle of the crack also impacts the strain magnitude, with larger angles resulting in smaller strain variations, and different crack angles of 0°, 45° and 90° can be distinguished.

The experimental results in this paper completely show that FBG sensors have excellent strain monitoring capability, which can be fully applied to strain monitoring and crack locations and

angles identification of wind turbine bolts in service. With the continuous progress of FBG sensing technology, its application in the field of wind power will become more and more extensive, providing a more solid guarantee for safe operation of wind turbines.

Acknowledgements

This work was supported by the Jiangsu Provincial Market Regulation Administration Science and Technology Project (No. KJ2022049 and No. KJ2024092), and by the Postgraduate Research & Practice Innovation Program of Yancheng Institute of Technology (No. KYCX_XZ050).

References

[1] Ma, L., Kong, X., Liu, X., Abdelbaky, M. A., Besheer, A. H., Wang, M., & Lee, K. Y. (2023). Offshore wind power generation system control using robust economic MPC scheme. *Ocean Engineering*, *283*, 115178. https://doi.org/10.1016/j.oceaneng.2023.115178

[2] Ran, M., Huang, J., Qian, W., Zou, T., & Ji, C. (2023). EMD-based gray combined forecasting model – Application to long-term forecasting of wind power generation. *Heliyon*, *9*(7), e18053. https://doi.org/10.1016/j.heliyon.2023.e18053

[3] Dziadak, B., Makowski, Ł., & Michalski, A. (2016). Survey of energy harvesting systems for wireless sensor networks in environmental monitoring. *Metrology and Measurement Systems*, *23*(4), 495–512. https://doi.org/10.1515/mms-2016-0053

[4] Sun, L., Yin, J., & Bilal, A. R. (2023). Green financing and wind power energy generation: Empirical insights from China. *Renewable Energy*, *206*, 820–827. https://doi.org/10.1016/j.renene.2023.02.018

[5] Liu, R., Dan, B., Zhou, M., & Zhang, Y. (2020). Coordinating contracts for a wind-power equipment supply chain with joint efforts on quality improvement and maintenance services. *Journal of Cleaner Production*, *243*, 118616. https://doi.org/10.1016/j.jclepro.2019.118616

[6] Zheng, D., Guo, H., Zhang, S., & Liu, Y. (2023). Study on fatigue performance of double cover plate through-core bolted joint of rectangular concrete-filled steel tube bundle wind turbine towers. *Journal of Constructional Steel Research*, *203*, 107830. https://doi.org/10.1016/j.jcsr.2023.107830

[7] Stałowska, P., Suchocki, C., & Zagubień, A. (2023). Application of terrestrial laser scanning measurements for wind turbine blade condition surveying. *Metrology and Measurement Systems*, 30(3), 403-422. https://doi.org/10.24425/mms.2023.146419

[8] Braithwaite, J., Iñigo Gómez Goenaga, Tafazzolimoghaddam, B., & Mehmanparast, A. (2020). Sensitivity analysis of friction and creep deformation effects on preload relaxation in offshore wind turbine bolted connections. *Applied Ocean Research*, *101*, 102225. https://doi.org/10.1016/j.apor.2020.102225

[9] Wagle, S., & Kato, H. (2009). Ultrasonic wave intensity reflected from fretting fatigue cracks at bolt joints of aluminum alloy plates. *NDT&E International*, *42*(8), 690–695. https://doi.org/10.1016/j.ndteint.2009.06.002

[10] Zhu, J. Z., Zhang, C. S., Feng, F. Z., Min, Q. X., & Xu, C. (2016). Study on probability of detection for fatigue cracks in sonic infrared imaging. *Infrared Physics Technology*, *77*, 296–301. https://doi.org/10.1016/j.infrared.2016.06.012

[11] Hasni, H., Jiao, P., Alavi, A. H., Lajnef, N., & Masri, S. F. (2018). Structural health monitoring of steel frames using a network of self-powered strain and acceleration sensors: A numerical study. *Automation in Construction*, *85*, 344–357. https://doi.org/10.1016/j.autcon.2017.10.022

[12] Liu, M., Yang, X., Song, H., Cai, Q., & Li, P. (2022). Single-peak fitting based on wavelength recognition in FBGs spectra under quadratic strain distribution. *Optical Fiber Technology*, *74*, 103136. https://doi.org/10.1016/j.yofte.2022.103136

[13] Chilelli, S. K., Schomer, J. J., & Dapino, M. J. (2019). Detection of crack initiation and growth using fiber Bragg grating sensors embedded into metal structures through ultrasonic additive manufacturing. *Sensors*, 19(22), 4917. https://doi.org/10.3390/s19224917

[14] Mieloszyk, M., & Ostachowicz, W. (2017). An application of Structural Health Monitoring system based on FBG sensors to offshore wind turbine support structure model. *Marine Structures*, *51*, 65–86. https://doi.org/10.1016/j.marstruc.2016.10.006

[15] Alamandala, S., Prasad, R. S., Pancharathi, R. K., Pavan, V. D. R., & Kishore, P. (2021). Study on bridge weigh in motion (BWIM) system for measuring the vehicle parameters based on strain measurement using FBG sensors. *Optical Fiber Technology*, *61*, 102440. https://doi.org/10.1016/j.yofte.2020.102440

[16] Ferro, C. G., Aimasso, A., Bertone, M., Sanzo, N., Dalla Vedova, M. D. L., & Maggiore, P. (2023). Experimental development and evaluation of a fiber Bragg grating-based outside air temperature sensor for aircraft applications. *Transportation Engineering*, *14*, 100214. https://doi.org/10.1016/j.treng.2023.100214

[17] Slah, R. K., Kumar, A., Gautam, A., & Rajak, V. K. (2022). Temperature independent FBG based displacement sensor for crack detection in civil structures. *Optical Fiber Technology*, *74*, 103137. https://doi.org/10.1016/j.yofte.2022.103137

[18] Dai, T. T., Jia, Z. G., Ren, L., & Li, Y. T. (2022). Design and experimental study on FBG-based crack extension monitoring sensor. *Optical Fiber Technology*, *71*, 102946. https://doi.org/10.1016/j.yofte.2022.102946

[19] Bao, X., Wang, Z., Fu, D., Shi, C., Iglesias, G., Cui, H., & Sun, Z. (2022). Machine learning methods for damage detection of thermoplastic composite pipes under noise conditions. *Ocean Engineering*, *248*, 110817. https://doi.org/10.1016/j.oceaneng.2022.110817

[20] Jin, X., Yuan, S. F., & Chen, J. (2019). On crack propagation monitoring by using reflection spectra of AFBG and UFBG sensors. *Sensors and Actuators A: Physical*, *285*, 491–500. https://doi.org/10.1016/j.sna.2018.11.052

[21] Zhang, W., Zhang, M., Lan, Y., Zhao, Y., & Dai, W. (2020). Detection of crack locations in aluminum alloy structures using FBG sensors. *Sensors*, *20*(2), 347. https://doi.org/10.3390/s20020347

[22] Sun, L. Y., Liu, C. C., Jiang, M. S., Zhang, L., Zhang, F. Y., Sui, Q. M., & Jia, L. (2021). Fatigue Crack Prediction Method for Aluminum Alloy Based on Fiber Bragg Grating Array. *Chinese Journal of Lasers, 48*(13), 1306003. https://doi.org/10.3788/CJL202148.1306003

[23] Yazdizadeh, Z., Marzouk, H., & Hadianfard, M. A. (2017). Monitoring of concrete shrinkage and creep using Fiber Bragg Grating sensors. *Construction and Building Materials*, *137*, 505–512. https://doi.org/10.1016/j.conbuildmat.2017.01.084

[24] Yao, Y., Tung, S. T. E., & Glisic, B. (2014). Crack detection and characterization techniques – An overview. *Structural Control and Health Monitoring*, 21(12), 1387–1413. https://doi.org/10.1002/stc.1655

[25] Buchukuri, T., Chkadua, O., & Natroshvili, D. (2021). Mixed- and crack-type dynamical problems of electro-magneto-elasticity theory. *Georgian Mathematical Journal*, *28*(4), 533–553. https://doi.org/10.1515/gmj-2020-2051

[26] Wang, H., Liu, X., Wang, X., & Wang, Y. (2019). Numerical method for estimating fatigue crack initiation size using elastic-plastic fracture mechanics method. *Applied Mathematical Modelling*, *73*, 365–377. https://doi.org/10.1016/j.apm.2019.04.010

[27] Zhao, H., Zeng, X., Chen, L., Pang, H., & Kou, H. (2020). Weight function solution of stress intensity factors for delayed hydride cracking of zirconium alloys. *Journal of Nuclear Materials*, *539*, 152206. https://doi.org/10.1016/j.jnucmat.2020.152206

[28] Ayatollahi, M. R., Bahrami, B., Mirzaei, A. M., & Yahya, M. Y. (2019). Effects of support friction on mode I stress intensity factor and fracture toughness in SENB testing. *Theoretical and Applied Fracture Mechanics*, *103*, 102288. https://doi.org/10.1016/j.tafmec.2019.102288

[29] Verma, V. K., Gopalakrishnan, C. K., Hamada, S., Yokoi, T., & Noguchi, H. (2021). Effect of strain localization on fatigue properties of precipitation-hardened steel with an arbitrarily length crack. *International Journal of Fatigue*, *143*, 106017. https://doi.org/10.1016/j.ijfatigue.2020.106017

[30] Hong, C., Yang, Q., Sun, X., Chen, W., & Han, K. (2021). A theoretical strain transfer model between optical fiber sensors and monitored substrates. *Geotextiles and Geomembranes*, *49*(6), 1539–1549. https://doi.org/10.1016/j.geotexmem.2021.07.003

[31] Isah, B. W., Mohamad, H., & Ahmad, N. R. (2021). Rock stiffness measurements fibre Bragg grating sensor (FBGs) and the effect of cyanoacrylate and epoxy resin as adhesive materials. *Ain Shams Engineering Journal*, *12*(2), 1677–1691. https://doi.org/10.1016/j.asej.2020.09.007

[32] Tian, H., Zhou, Z., Li, B., & Jiang, C. (2023). Effect of strain gradient on the stress-strain relationship of FRP-confined ultra-high performance concrete. *Composite Structures*, *304*, 116371. https://doi.org/10.1016/j.compstruct.2022.116371

[33] Fu, G., Zhou, S., & Qi, L. (2020). On the strain gradient elasticity theory for isotropic materials. *International Journal of Engineering Science*, *154*, 103348. https://doi.org/10.1016/j.ijengsci.2020.103348

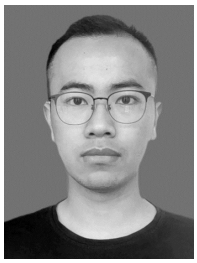

Yutao Chen received the B.Sc. degree from Changshu Institute of Technology, China, in 2022. He is a full-time graduate student in Yancheng Institute of Technology, majoring in mechanical automation, with his main focus on structural health monitoring.

Peng Zhou received the B.Sc. degree from Yancheng Institute of Technology, China, in 2008. He is currently an Assistant Engineer of Yancheng Institute of Supervision & Inspection of Product Quality. His main research interest is mechanical testing.

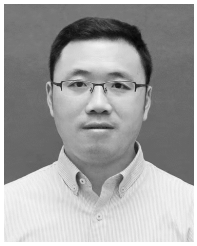

Liyun Chen received the M.Sc. degree from Nanjing Technical University, China, in 2009. He is currently a Senior Engineer of Yancheng Institute of Supervision & Inspection of Product Quality. His main research interest is mechanical testing and NDT.

Liya Dai received the B.Eng. degree from Baicheng Normal University, China, in 2023. She is a full-time graduate student at Yancheng Institute of Technology, majoring in civil and hydraulic engineering, with her main focus on structural health monitoring.

Guoqing Gu received the Ph.D. degree from Nanjing University of Aeronautics & Astronautics, China, in 2013. He is currently an Associate Professor of the School of Civil Engineering of Yancheng Institute of Technology. His research activity focuses on experimental mechanics.

Yongqing Wang received the Ph.D. degree from Nanjing University of Science and Technology, China, in 2017. He is currently a lecturer of Yancheng Institute of Technology. His main research interest is industrial automation testing and photoelectric detection.